Investigation of deformation induced precipitation and the related microstructure evolution of Al–Zn–Mg–Cu alloy

To cite this article: Jinrong Zuo *et al* 2020 *Mater. Res. Express* **7** 106529

Materials Research Express

PAPER

Investigation of deformation induced precipitation and the related microstructure evolution of Al–Zn–Mg–Cu alloy

Jinrong Zuo[1,2,*], **Longgang Hou**[3], **Xuedao Shu**[1,2], **Wenfei Peng**[1,2], **Anmin Yin**[1,2] and **Jishan Zhang**[3]

[1] College of Mechanical Engineering and Mechanics, Ningbo University, Ningbo 315211, People's Republic of China
[2] Zhejiang Provincial Key Laboratory of Part Rolling Technology, Ningbo 315211, People's Republic of China
[3] State Key Laboratory for Advanced Metals and Materials, University of Science and Technology Beijing, 30 Xueyuan Road, Haidian District, Beijing 100083, People's Republic of China
[*] Author to whom any correspondence should be addressed.

E-mail: shuxuedao@nbu.edu.cn, pengwenfei@nbu.edu.cn, yinanmin@nbu.edu.cn, lghou@skl.ustb.edu.cn, zhangjs@skl.ustb.edu.cn and zuojinrong@nbu.edu.cn

Keywords: Al–Zn–Mg–Cu, deformation, $MgZn_2$, precipitates, microstructure

OPEN ACCESS

RECEIVED
10 September 2020

REVISED
9 October 2020

ACCEPTED FOR PUBLICATION
16 October 2020

PUBLISHED
30 October 2020

Abstract

As heating time, temperature, strain and strain rate are the four most commonly used controllable parameters in thermomechanical treatments of high strength aluminum alloy, which have great influence on microstructures and mechanical properties. 7055 Al alloy was subjected to solution and thermomechanical treatment (4 routes) at different heating time (route 1), temperatures (route 2), strains (route 3) and strain rates (route 4) to investigate their effects on grain structure and precipitation. The results show that $MgZn_2$ particles are almost completely dissolved back into the matrix after solution treatment, but the coarse Al_7Cu_2Fe and Al_2CuMg remain steady. Particles preferentially precipitate at grain boundaries. Precipitates free zones appear after aging at 300 °C for different time in route 1. With the increased over aging time, precipitates grow and the quantity of rod-shaped increases. After hot deformation, grains are elongated and numerous deformation induced precipitates are formed. Grain width increases with the increase of strain temperature/rate in route 2 and route 4. However, with further strain, grain width first decreases and then increases with the minimum value taken at 60% deformation in route 3. Due to the effect of deformation on spheroidization and refinement of precipitates, the size of precipitates decreases with strain and is spheroidized gradually in route 2 compared with route 1. Strain energy plays the dominant role during over aging or at low strain leading the rod liked precipitates, with the increase of strain, interfacial energy plays the decisive role, and precipitates are spherical.

1. Introduction

With the development of modern industry (especially aerospace), the comprehensive properties requirement of high strength aluminum alloy is higher and higher [1]. But the existing micro alloying and heat treatment cannot satisfy the need of modern industry. High strength, toughness, corrosion resistance and damage tolerance indubitably become the main development direction of Al–Zn–Mg–Cu alloys [2]. Therefore, improving the ductility of the alloy by optimizing microstructures while maintaining high strength has become an important and urgent issue.

Former research on deformation of aluminum alloy mainly focused on deformation mode (e.g., conventional deformation (rolling, extrusion, forging) and sever plastic deformation (Equal channel angular extrusion, multi direction forging, cryogenic rolling)), the influence of deformation parameters [3–5], the evolution of micostructures (dislocation, subgrain and deformation band, etc) [6, 7], and the control of recrystallization structure [8]. Wert *et al* [9]. introduced large/small precipitates into 7075 Al alloy by over aging at high temperature to improve microstructures. By which grains were refined effectively. Since then, precipitation of the second phase particles has become one of the hottest spots in the research of Al–Zn–Mg–Cu

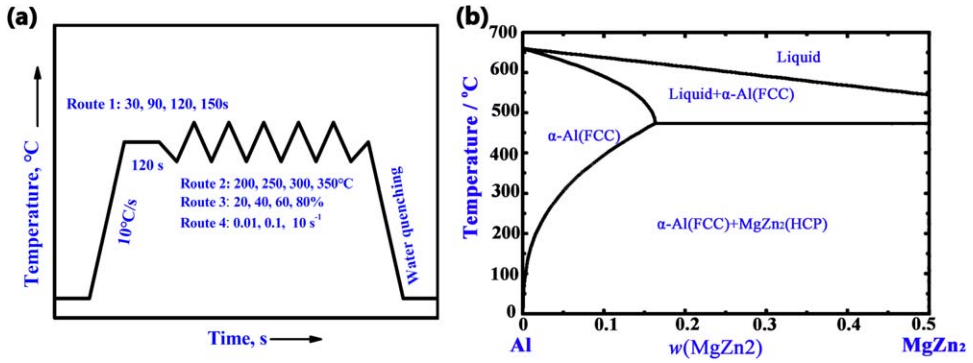

Figure 1. (a) Schematic presentations of compression processing; (b) Phase diagram of Al-$MgZn_2$ system.

alloys. Recently, it has been found that spheroidization of $MgZn_2$ particles can be achieved by ECAP (Equal channel angular pressing) [10] and deformation induced precipitation (DIP) treatment [11]. These $MgZn_2$ affects deformed microstructure and improves mechanical properties of the alloy. The re-precipitation and re-dissolution of precipitates can also be induced in Al-Cu alloy during SPD (severe plastic deformation). The precipitation, coarsening, crushing and spheroidization of precipitates are also accompanied by the ECAP process in Al–Zn–Mg–Cu alloy [12–14]. The quantity, morphology, size and distribution of precipitates significantly affect grain structure evolution and boundaries migration of Al alloy, thus improving the microstructure and mechanic properties. However, previous studies on precipitates of Al–Zn–Mg–Cu alloy mainly focused on SPD at room temperature or artificial aging process, but the composite effect of temperature and deformation on precipitation is also very important. Therefore, in this paper, the precipitation behavior of the second phase during thermomechanical treatment was studied. Precipitates were introduced by over aging or hot deformation. Grain evolution and dynamic precipitation behavior of nano $MgZn_2$ particles with different parameters were also investigated.

2. Materials and methods

As hot rolled commercial 7055 Al alloy plates (HR-7055 chemical composition: 8.38Zn–2.07Mg–2.31Cu–0.13Zr–0.16Ti–0.092Fe–0.056Si (wt%)) were solution treated at 470 °C for 16 h plus 475 °C for 8 h in air furnace and rapidly quenched into room-temperature water with quenching transfer time less than 5 s (marked as SQ-7055). Then the plates were machined into cylindrical samples with diameter of 10 mm and length of 15 mm. The cylindrical samples for hot compression were taken from the center of hot rolled plates (HR-7055). The hot compression deformation direction is consistent with the original hot rolling direction. Two ends of the cylinder were milled and polished.

Hot compression experiment was carried out on a thermal simulator (DSI Gleeble−3500). Graphite powder and oil were coated on the two end faces of the cylindrical sample as the lubricant to reduce the influence of friction force during compression. The thermomechanical treatment process is shown in figure 1(a) and table 1. Route 1: samples were heated to 300 °C and held for 30∼150 s (OV-30∼OV-150). SQ-7055 needs to be heated and held for a certain time before deformation to ensure that temperature of the alloy is uniform. Which can be treated as a special over aging process. In this study, the over aging treatment before hot deformation can not only ensure the temperature uniformity of SQ-7055, but also obtain appropriate size and density of precipitates to pin dislocations and boundaries, which is conducive to the subsequent thermomechanical treatment to increase the deformation storage energy. Simultaneously, the over aging process can also be treated as a comparative experiment (heating *versus* heating + deformation), eliminating the interference of heating to study the influence of strain on precipitation. Route 2 (effect of deformation temperature on microstructures): samples were heated to 200 °C∼350 °C for 120 s and deformed at strain rate of 0.1 s^{-1}, sample height was reduced from 15 mm to 6 mm, 60% reduction (DIP-T200∼DIP-T350). Route 3 (effect of strain on microstructures): heated to 300 °C for 120 s and deformed at strain rate of 0.1 s^{-1}, sample height was reduced from 15 mm to 12∼3 mm, 20∼80% reduction (DIP-D20∼DIP-D80). Route 4 (effect of strain rate on microstructures): After heating to 300 °C and holding for 120 s, specimens were deformed at strain rate of 0.01∼10 s^{-1}, 60% reduction (DIP-R0.01∼DIP-R10). The heating rate of all samples was 2 °C s^{-1} and all samples were water quenched at room temperature immediately after deformation or heat treatment to retain the high-temperature deformation structure. The pseudo binary system of Al-$MgZn_2$ is shown in figure 1(b). It can be seen that the solubility of $MgZn_2$ in Al matrix increases slowly with temperature (<300 °C), but it increases

Table 1. Specific parameters of compression process.

Route	Process	T, °C	t, s	$\dot{\varepsilon}$, s^{-1}	ε, %	Height, mm
Route 1	OV-30	300	30	—	—	—
	OV-90	300	90	—	—	—
	OV-120	300	120	—	—	—
	OV-150	300	150	—	—	—
Route 2	DIP-T200	200	120	0.1	60	15 → 6
	DIP-T250	250	120	0.1	60	15 → 6
	DIP-T300	300	120	0.1	60	15 → 6
	DIP-T350	350	120	0.1	60	15 → 6
Route 3	DIP-D20	300	120	0.1	20	15 → 12
	DIP-D40	300	120	0.1	40	15 → 9
	DIP-D60	300	120	0.1	60	15 → 6
	DIP-D80	300	120	0.1	80	15 → 3
Route 4	DIP-R0.01	300	120	0.01	60	15 → 6
	DIP-R0.1	300	120	0.1	60	15 → 6
	DIP-R10	300	120	10	60	15 → 6

OV-over aging, DIP-deformation induced precipitate, T- deformation temperature, t-holding time, $\dot{\varepsilon}$-strain rate, ε-strain.

rapidly above 300 °C. Therefore, the precipitation of $MgZn_2$ from metastable supersaturated solid solution is a spontaneous thermodynamic process. The deformation temperature was set at (200 °C∼350 °C) to study the effect of temperature on precipitates. And the corresponding over aging contrast tests (300 °C for different time) were also carried out.

Microstructures (Grain, precipitates, orientation, etc) evolution was analyzed by optical microscope (OM, Zeiss MC80DX), scanning electron microscopy (SEM ZEISS-ULTRA55 with EDS (energy dispersive spectrometer) and EBSD (electron back scattering diffraction), transmission electron microscopy (TEM, Hitachi H800 and JEOL Ltd JEM2010). The standard metallographic specimen preparation method was used, and the etching reagent is Keller's reagent (2.5% HNO_3 + 1.5% HCl + 1% HF aqueous solution). In EBSD maps, black thick lines represent HAGBs (high Angle grain boundaries, $\theta > 15°$), while the gray thin lines represent LAGBs (low Angle grain boundaries, $2° < \theta < 15°$). After mechanical polishing, the sample surfaces were electropolished with 70% methanol and 30% nitric acid solution at −30 °C and 30 V voltage to remove the deformed layer. Samples were installed on a pre-titled sample holder with an tilt angle of 70°, acceleration voltage of 20 kV, step size of 1 μm, and coverage area of approximately 0.12 mm^2. To consider the statistics, three such random regions were examined. TEM films were thinned by twin-jet electropolishing device. The electrolyte was 30% nitric acid and 70% methanol (volume fraction), the current was 50∼70 mA, and temperature was −20∼30 °C. OM, SEM, EBSD and TEM samples were all cut from LD-ND (longitudinal direction and normal direction) (cross-section) of the deformed 7055 Al alloy center. The size and area fraction of the second phase were analyzed by 'Image J' software in SEM or TEM images. In order to reduce the effect of error, 3 random SEM/TEM images were taken as the average value. It is difficult to measure the volume fraction of precipitates directly, which can be calculated by the area fraction. According to Delesse theorem [15]. In 7055 Al alloy, take the cube with side length L, and place X, Y, Z coordinates on the cube. The volume V_{MgZn2} of $MgZn_2$ phase in the cube can be expressed as follows:

$$V_{MgZn_2} = \int_0^L A_{MgZn_2} L^2 dy \tag{1}$$

Where A_{MgZn2} is the area fraction of $MgZn_2$ measured on any cross section, which changes with the position of cross section (i.e. Y coordinate). It can be seen from formula (1) that the volume fraction of $MgZn_2$ is positively related to its area fraction (volume fraction increases with the increased area fraction).

3. Results and discussion

3.1. Microstructure of plates after double-step solution treatment

In Al–Zn–Mg–Cu alloys, η ($MgZn_2$) and T ($Al_2Mg_2Zn_3$) phases were formed by the combination of Zn and Mg. The solubility of these two phases in Al–Zn–Mg–Cu alloys is very high, and changes sharply with temperature. The solubility of the former is 4%–5% at 300 °C. Cu forms S (Al_2CuMg) phase with other elements.

Figure 2(a) shows microstructure of the initial HR-7055 alloy. It can be seen that the initial grains are coarse, second phase particles appear in grain interior and boundaries, while that at grain boundaries are coarser. The

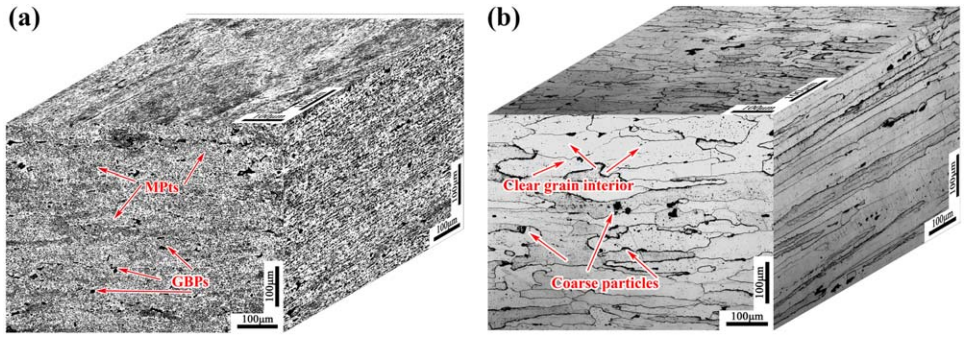

Figure 2. 3D-OM of 7055 Al alloy: (a) for HR-7055; (b) for SQ-7055.

cavities in figure 2 are the holes left by the second phase particles falling off during mechanical polishing or etching.

In the initial state of HR-7055 Al alloy, there are abundant $MgZn_2$, Al_2CuMg, Al_7Cu_2Fe and Al_3Zr due to its manufacturing process (casting, homogenization, hot rolling). In order to make the research meaningful, the initial alloy should return to the homogenization state before hot deformation, that is, solid solution alloy with uniform microstructure and no segregation. Simultaneously it is also necessary to ensure that the alloy does not over-burn. Therefore, how to determine the solution temperature becomes the first step in this study

According to the temperature-precipitates diagram of Al–Zn–Mg–Cu alloy [16] and the correlation constants of main precipitates [17, 18], it can be seen that the volume fraction of M phase (i.e. $MgZn_2$) gradually decreases, while that of S-Al_2CuMg phase increases gradually in the range of 210~435 °C; the volume fraction of S phase decreases gradually in the range of 435~470 °C. That means Al–Zn–Mg–Cu alloy can be regarded as single-phase solid solution in the temperature range of 470–490 °C; however, when temperature is higher than 490 °C, liquid phase appears, i.e., overburning occurs. Therefore, the optimal solution temperature should be between 470 °C and 490 °C (the interval of single-phase solid solution). Detailed solution treatment parameters are shown in table 2.

After solution treatment, grains grow slightly, larger than 600 μm in longitudinal and 200 μm in transverse. No obvious overburning phenomenon (no spherical eutectic structure in the matrix or grains, and no melted black triangle at the junction of three grains [19]) appears. Grain interior is clearer for redissolved precipitates. There are still some insoluble coarse second phase particles at grain boundaries (figure 2(b)).

It can be seen from the SEM images that plenty of coarse spherical particles, fine needle like particles and fishbone like particles appear in HR-7055 alloy (figures 3(a) and (b)). EDS results (table 3) show that the fishbone like second phase in figure 3(a) is iron rich phase (Al_2Cu_7Fe) (marked as A); the coarse elliptical second phase in figure 3(b) is S phase (Al_2CuMg) (marked as B); and the relatively small needle liked second phase in figure 3(b) is $MgZn_2$ phase (marked as C). The size of $MgZn_2$ particles here has reached micron level losing the strengthening effect. In order to make 7055 Al alloy single-phase solid solution with uniform structure and no segregation, the plates need special solution treatment.

Still two kinds of second phase particles exist in the alloy after solution treatment ((figures 3(c), (d))): coarse hollow fishbone particles D and coarse spherical particles E. The edge of particle E is more rounded, which indicates partial redissolution during the double-step solution, while the fishbone like phase D has no obvious change. In figures 3(c), (d), almost no needle like $MgZn_2$ particles can be observed, which indicates these particles have been decomposed in the long-term solid solution and fully redissolved into the matrix. According to EDS analysis in table 3, the hollowed fishbone like second phase particles D in figure 3(c) are iron rich phase, and the coarse spherical particles E in figure 3(d) are S phase. It has been proved that these two phases can not be fully redissolved in the solid solution treatment with prolonged high temperature solution time [20]. Furthermore, it may lead to the aggregation of these particles along grain boundaries, which may have a negative impact on the mechanical properties and corrosion resistance [21].

The distribution of HAGBs (high angle grain boundaries) and LAGBs (low angle grain boundaries) of HR-7055 and SQ-7055 are shown in figure 4. Obvious recrystallization occurs in SQ-7055, no LAGBs with gray thin lines appear in the recrystallized grains interior. It can be seen from IPF diagram that grain orientation distribution of SQ-7055 is more random compared with that of HR-7055 and the recrystallization volume fraction is about 28.6%. High-density LAGBs appear in the elongated grains. The distribution of grain boundary misorientation is also calculated in figures 4(a3) and (b3). Compared with HR-7055 Al alloy, grains of SQ-7055 are further recrystallized with the increased HAGBs, refined and more uniformly distributed grains.

Table 2. Double-step solution treatment parameters of 7055 Al alloy.

Heating rate °C min^{-1}	Solution temperature of the first step, °C	holding time, h	Heating rate, °C min^{-1}	Solution temperature of the second step, °C	Holding time, h	Quenching and cooling mode
2	470	16	0.1	475	8	Room temperature water cooling

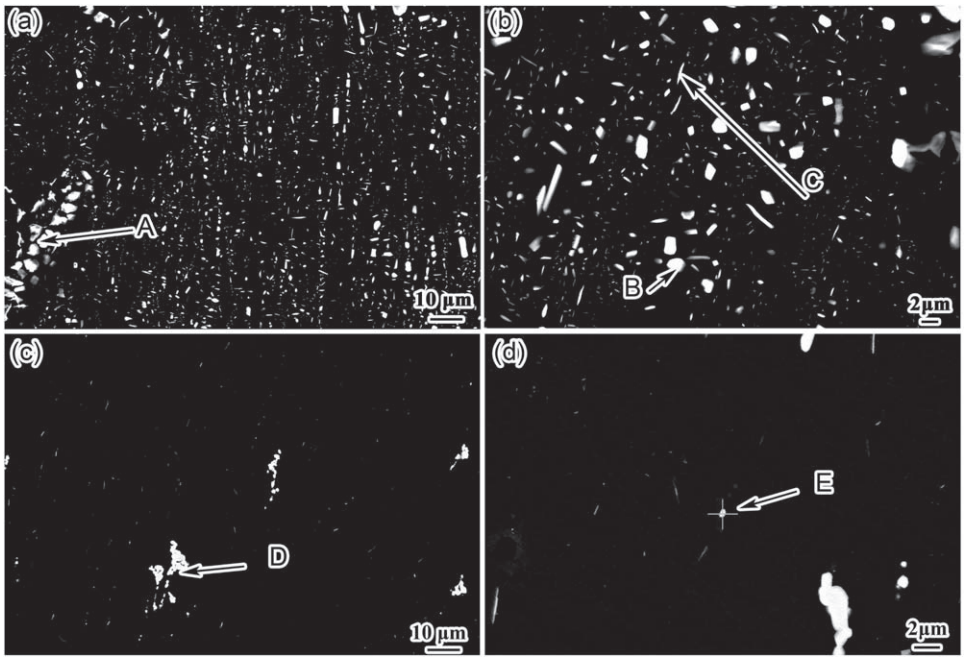

Figure 3. SEM images of 7055 Al alloy: (a), (b) for HR-7055 and (c), (d) for SQ-7055.

Table 3. EDS results of the labeled particles in figure 3.

(a)

Element Line	Weight %	Weight % Error	Atom %	Atom Error
Al K	58.15	+/-0.17	76.13	+/-0.22
Fe K	13.26	+/-0.2	6.79	+/-0.23
Cu K	30.59	+/-0.17	17.08	+/-0.09
Total	100		100	

(b)

Element Line	Weight %	Weight % Error	Atom %	Atom Error
Mg K	16.01	+/-0.12	75.12	+/-0.15
Al K	39.05	+/-0.19	7.78	+/-0.21
Cu K	44.94	+/-0.13	17.00	+/-0.06
Total	100		100	

(c)

Element Line	Weight %	Weight % Error	Atom %	Atom Error
Mg K	16.01	+/-0.12	75.12	+/-0.15
Al K	39.05	+/-0.19	7.78	+/-0.21
Cu K	44.94	+/-0.13	17.00	+/-0.06
Total	100		100	

(d)

Element Line	Weight %	Weight % Error	Atom %	Atom Error
Al K	58.15	+/-0.17	76.13	+/-0.22
Fe K	13.26	+/-0.2	6.79	+/-0.23
Cu K	30.59	+/-0.17	17.08	+/-0.09
Total	100		100	

(e)

Element Line	Weight %	Weight % Error	Atom %	Atom Error
Mg K	16.01	+/-0.12	75.12	+/-0.15
Al K	39.05	+/-0.19	7.78	+/-0.21
Cu K	44.94	+/-0.13	17.00	+/-0.06
Total	100		100	

3.2. Evolution of precipitates during over aging

There are mainly three kinds of second phase particles in 7xxx series Al alloys [22]. The first is coarse particle with size $>$ 0.6 μm and contains elements such as Fe, Si, Cu, etc; the second with intermediate size, between 0.02 μm and 0.6 μm, which is dominated by the dispersed phase containing Cr, Mn, Zr, etc, and the last is fine precipitates with size less than 0.5 μm (e.g., $MgZn_2$). The former two kinds of particles are high melting point precipitates produced during casting, which changes little during the subsequent heat treatment and hot working [9], while the last is aging precipitation strengthening phase, which can precipitate, redissolve and re-precipitate in heat treatment and hot deformation [21, 23]. The precipitation of $MgZn_2$ from metastable α-Al solid solution is a spontaneous thermodynamic process under liquidoid. The driving force $\Delta G^{\alpha\rightarrow\alpha'+\eta}$ is enough to promote the precipitation of $MgZn_2$ from matrix.

In order to study the effects of strain on dynamic precipitation, comparative tests were set up to observe the precipitation process during over aging at corresponding temperatures. The cylindrical samples were heated to 300 °C at a rate of 2 °C s^{-1}, holding for 30~150 s, and then quenched with room temperature water immediately, so as to retain the over aged microstructure.

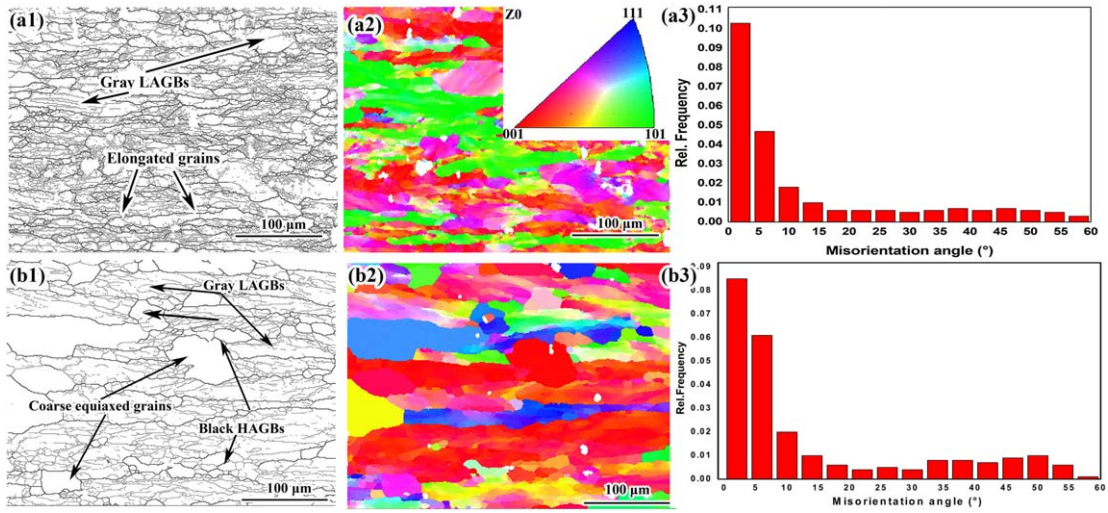

Figure 4. EBSD of (a) HR-7055 and (b) SQ-7055: (a1), (b1) for GB (grain boundary), (a2), (b2) for IPF (inverse pore figure) maps and (a3), (b3) for statistical images of misorientation angle.

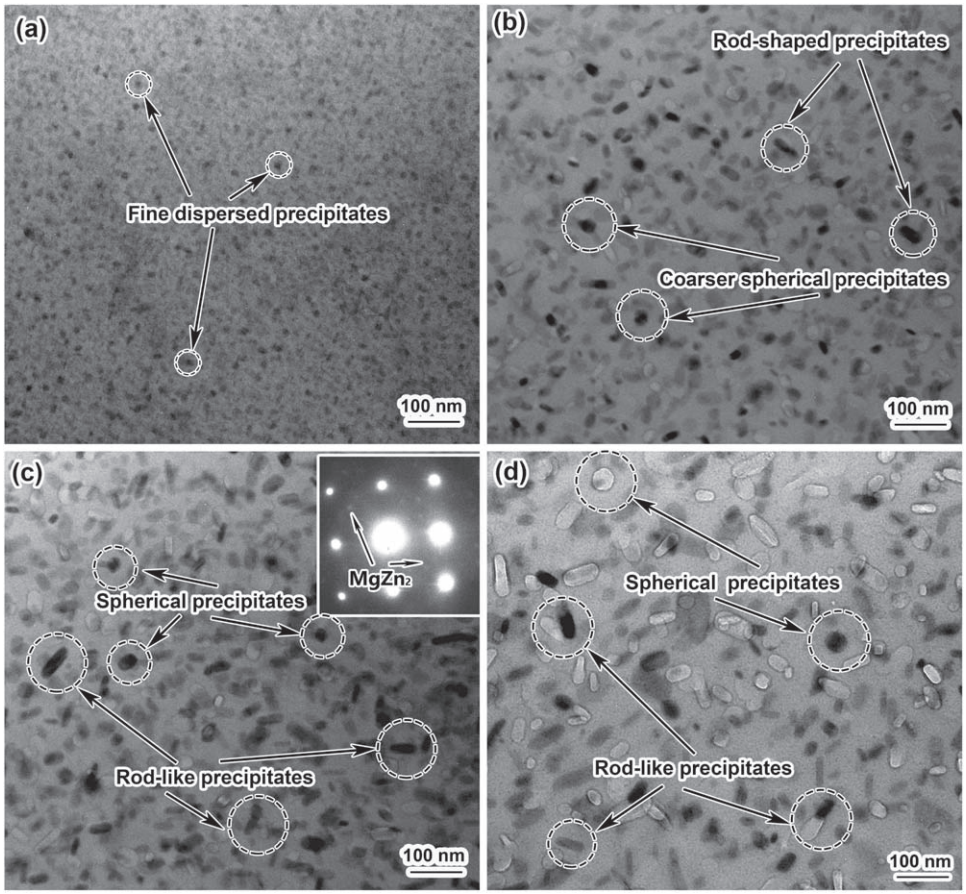

Figure 5. TEM of over aged 7055 Al alloy: (a) OV-30; (b) OV-90; (c) OV-120 with the corresponding SAED (the selected area electron diffraction) pattern inseted; (d) OV-150.

Figure 5 shows the evolution of precipitates after over aging at 300 °C. After 30 s, fine and uniformly distributed particles appeared in the alloy matrix (figure 5(a)); after 90 s, precipitates grew up obviously, while their distribution was still uniform with increased area fraction (figures 5(a), (b)); when the over aging time continued to increase to 120 s, precipitates further grew, and the rod-shaped dominated (figure 5(c)), which is verified as mainly $MgZn_2$ by SAED (the selected area electron diffraction) pattern in figure 5(c).

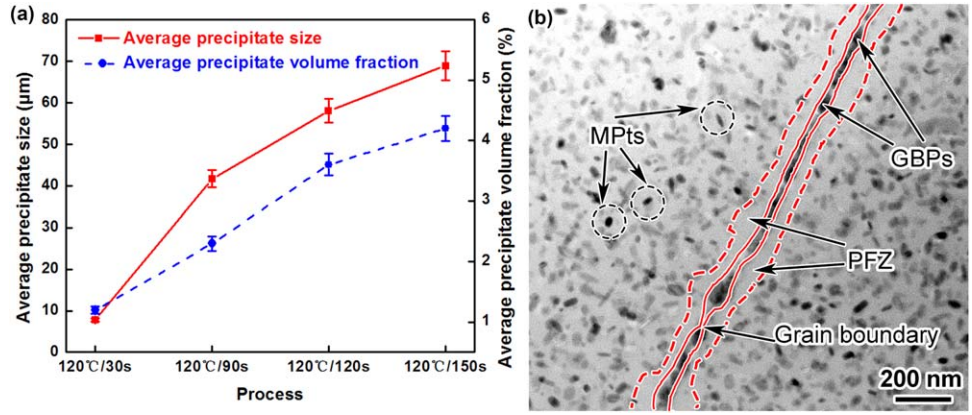

Figure 6. (a) Average size and fraction of precipitates after over aging treatment; (b) fine MPts, coarse continuous GBPs and wide PFZ of OV-120.

The pinning force of precipitates on boundaries can be expressed as [24]:

$$P_Z = 3F_V\gamma_b/d \tag{2}$$

P_Z: Zener drag force, F_V: volume fraction of precipitates, γ_b: constant, d: average diameter of precipitates.

Finally, when the over aging time increases to 150 s, precipitates grew up obviously (increased d), but their density decreased.

It can be seen from the statistical diagram in figure 6(a) that the volume fraction (F_V) of precipitates changes slowly after 120 s. Therefore, The drag force of precipitates decreases significantly [24] (figure 5(d)). The best route 1 for obtaining the optimized precipitate is obtained as follows: heated to the required temperature and held for 120 s to acquire precipitates with good pinning ability.

The MPts (matrix precipitates) and GBPs (grain boundary precipitats) are significantly different after 120 s over aging treatment (figure 6(b)). MPts are relatively finer and evenly distributed, while GBPs are larger and continuously distributed. Wide precipitate free zone appear between grain boundaries and MPts (the area between the dotted line and the solid line in figure 6(b)). T Ogura [25] quantitatively study the PFZ (precipitates free zone) in Al-Zn-Mg(-Ag) alloys by microchemical analysis and nanoindentation measurement to summarize the formation mechanism of PFZ. According to the research of Ogura T, the formation of PFZ in figure 6(b) may be explained as follows. The vacancy concentration near grain boundaries is lower than the critical nucleation concentration, which results in the failure of nucleation in the region. Furthermore, the low concentration of solute near the grain boundary leads to the decrease of supersaturation required for precipitation.

3.3. Microstructure analysis and dynamic precipitation evolution during hot deformation

Figure 7 shows grain structure and size statistics of 7055 Al alloy after hot compression deformation. It can be seen that grains of 7055 Al alloy were obviously elongated after deformation, and the transverse size was smaller than that of the SQ-7055 in figure 2(b). Some coarse second phase particles were crushed and discontinuous along grain boundaries after hot compression. With the increased deformation temperature (figures 7(a)–(d)), dynamic recovery become more and more serious, grain boundaries were straighter with wider and uneven spacing. High stacking fault energy and pinning of dispersed precipitates lead to no obvious dynamic recrystallization even after 350 °C hot deformation.

Figures 7(e)–(h) shows that with the increase of strain, partial coarse second phase particles are gradually crushed, grain width first decreased and then increased with the minimum value at 60% deformation (figures 7(g), (m)). After 40% deformation, grains were obviously elongated. With the increase of deformation (40%~80%), grains were gradually refined along the transverse direction to form long strip, namely deformation bands. The reason is that increased strain leads to serious dislocation stacking. The very short compression deformation time and large strain make it difficult for dislocation to slip, resulting in uneven deformation and forming deformation bands [26]. Moreover, no obvious dynamic recrystallization occurred in DIP-20~DIP-80, for the fast deformation rate, low deformation temperature, small deformation amount and high stacking fault energy. When deformation reaches 60% (DIP-60), grains are elongated along the compression direction and continuous 'wavy' structure appeared (figure 7(g)). The 'wavy' structure was caused by the fluctuation of flow stress in different regions after being elongated [27].

Figures 7(I)–(k) shows the microstructure after compression at different strain rates (DIP-R0.01~DIP-R10). It can be seen that when deformation rate is slow (0.01 s^{-1}), fine grains appeared near the original grain

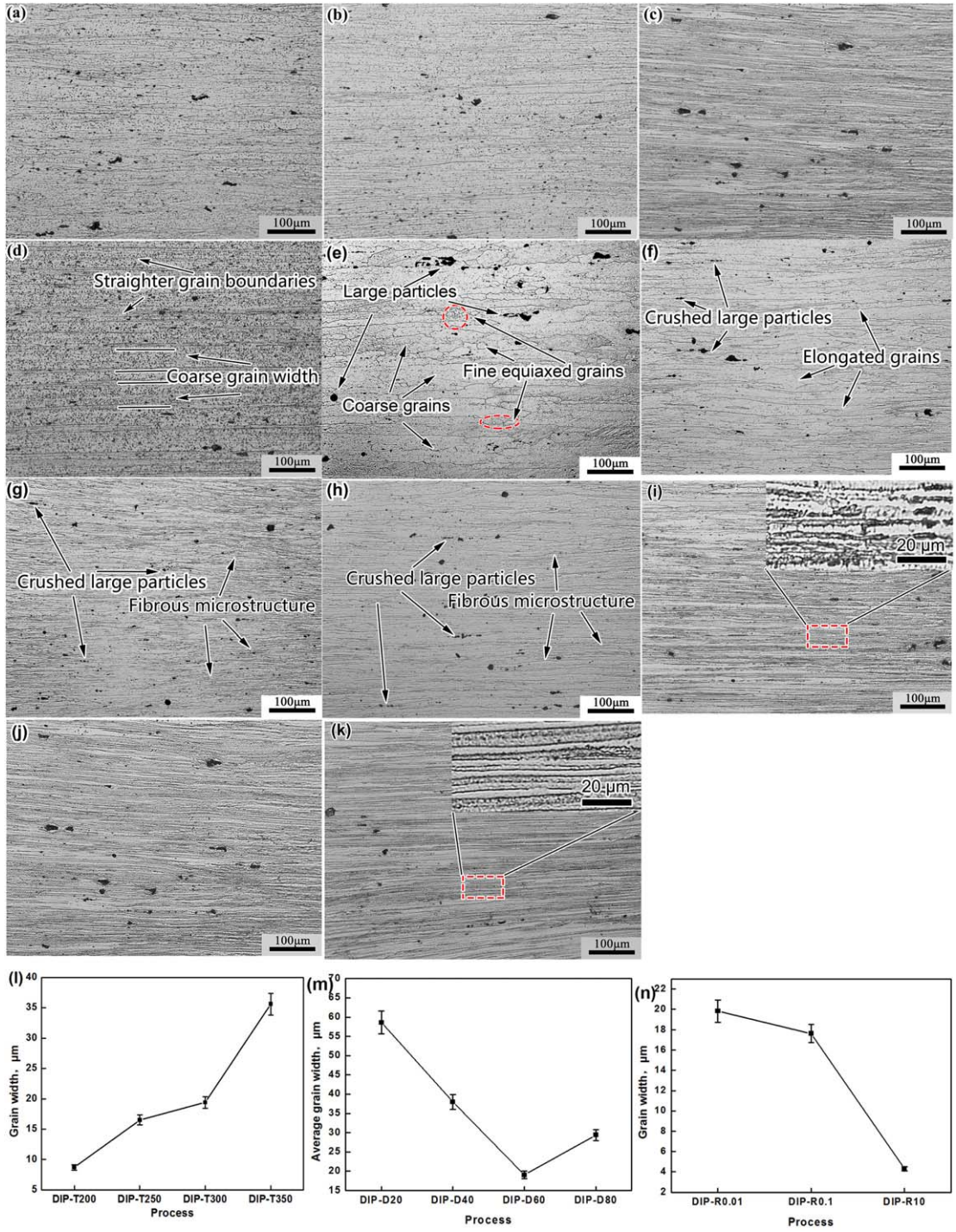

Figure 7. OM of 7055 Al alloy after deformation: (a) DIP-T200; (b) DIP-T250; (c) DIP-T300; (d) DIP-T350; (e) DIP-D20; (f) DIP-D40; (g) DIP-D60; (h) DIP-D80; (i) DIP-R0.01; (j) DIP-R0.1; (k) DIP-R10; (l)–(n) average grain width.

boundaries, which is dynamic recrystallization structure, and such fine grains decreased with the increased strain rate. Combined with figures 7(I)–(k) and (n), it can be seen that with the increased strain rate, grain boundary spacing become narrower and grain interior become clearer, indicating that the dynamic recovery/recrystallization decrease. The increase of strain rate leads to serious dislocation stacking, and short-term deformation makes dislocation slip difficult and uneven, resulting in deformation bands. Therefore, high strain rate is not conducive to the thermal activation and dislocation mobility, thus reducing the dynamic recovery/recrystallization.

The precipitation and growth of second phase particles during hot deformation not only involves thermodynamics, but also dynamics. Thermodynamics is the premise of precipitation, while dynamics can affect the parameters of precipitates, such as rate, morphology, size, density etc. Deformation storage energy E is

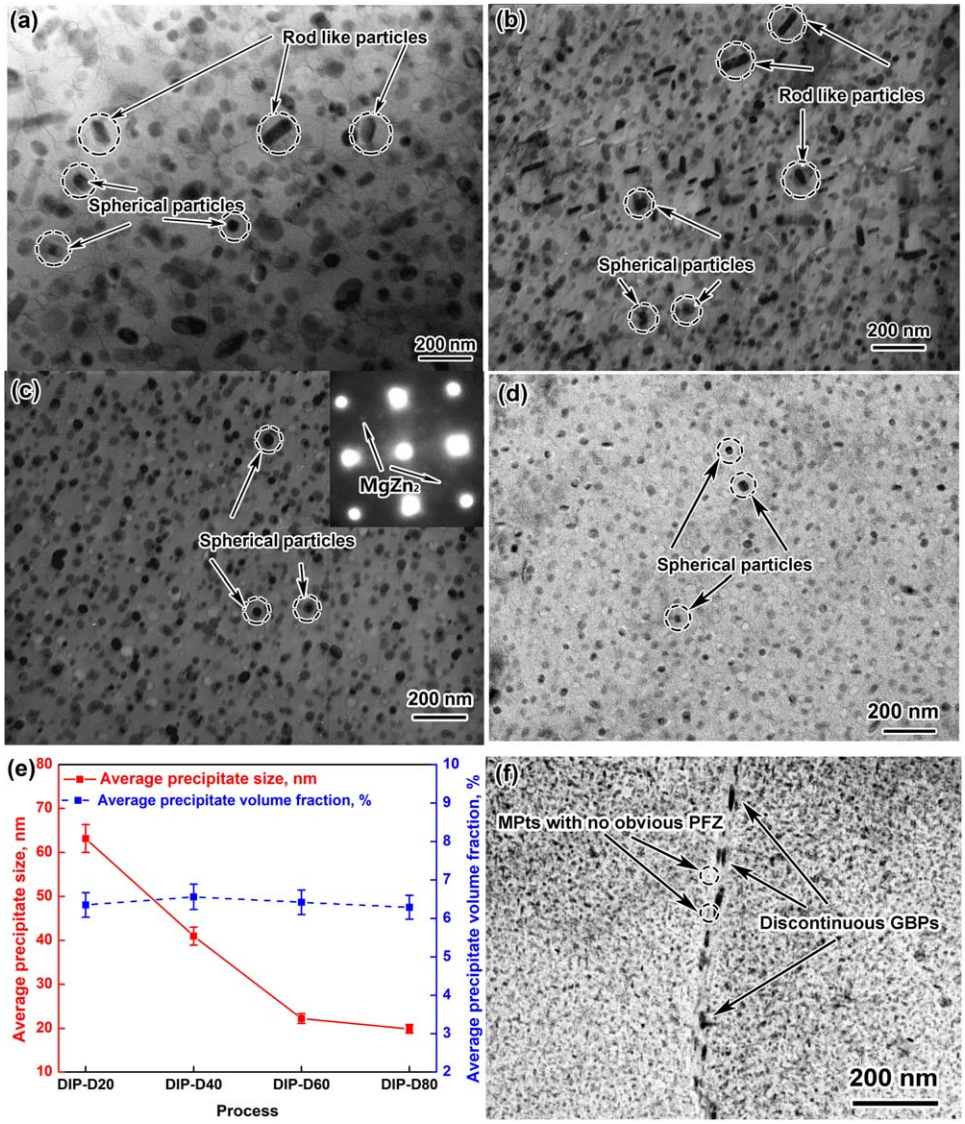

Figure 8. TEM images of DIPs: (a) DIP-D20; (b) DIP-D40; (c) DIP-D60 (the inset is the corresponding SAED pattern); (d) DIP-D80; (e) average sizes and fractions of precipitates; (f) discontinuous GBPs of DIP-D80.

introduced by strain. The driving force (Gibbs free energy of system) of $MgZn_2$ precipitation during deformation is as follows: $\Delta G_m^{\alpha\to\alpha'+\eta} - E$. The driving force for precipitation is greater than the equilibrium desolvation driving force of $MgZn_2$, so deformation is conducive to the nucleation of precipitates, and more $MgZn_2$ particles are precipitated than in equilibrium state during a certain period of time.

Troeger L P [28] found that deformation bands in figure 7 can also provide favorable sites for the heterogeneous nucleation of precipitates and affect their morphology. Precipitation and growth of the second phase particles are essentially the process of atomic diffusion, which leads to the segregation of elements. Plenty of defects (e.g., dislocations) were introduced by hot deformation, which can provide more nucleation sites for precipitates. Simultaneously, it can provide a great diffusion channel for solute atoms, accelerating atomic diffusion and promoting the precipitation and growth of $MgZn_2$.

Figure 8 shows the TEM images of precipitates after route 3. The density of precipitates increases with strain, and spheroidization of precipitates become more and more obvious. Figure 8(e) shows that with the increased strain, the volume fractions of precipitates change little, while their sizes refined greatly. Moreover, the quantity of rod-shaped precipitates decrease, while the spherical increase. The microstructure here is different from that of the over aged alloy (only heating in figure 5). Precipitates are more (increased density), refined and spheroidized by deformation. Such special precipitates are defined as deformation induced precipitates (DIPs) [29]. In the same way, the DIPs are also proved to be $MgZn_2$ phase by SAED pattern in figure 8(c). According to formula (2), the pinning force P_z increased with decreased precipitate size d and increased volume fraction F_V. which may retard the migration of boundaries to increase deformation storage energy and refine grains in some practical thermomechanical treatment [24].

It can be seen from figure 8(f) that the PFZ of DIP-80 is narrower than that of the over aged sample (OV-120 in figure 6(b)). The corrosion potentials of η' phase, PFZ and Al matrix are −0.869 V, −0.57 V and −0.68 V, respectively [22]. It is obvious that the corrosion potential of PFZ is higher than that of η' phase and aluminum matrix. In corrosive environment, both η' phase and aluminum matrix around PFZ will become anode and dissolve preferentially. Therefore, reducing the width of PFZ is beneficial to improve the corrosion resistance of the 7055 Al alloy [30].

3.4. Modeling of DIP

Through the above study on deformation induced precipitation, it is found that $MgZn_2$ spheroidized at a low strain ($\varepsilon = 0.9$, 60% warm deformation). There are different explanations for the phenomenon that deformation can spheroidize precipitates in Al–Zn–Mg–Cu alloy. Nam C Y [31] believed that in 7050 Al alloy, the coarse rod-shaped precipitates were crushed and spheroidized by ECAP at 250 °C. However, Sha G [32] thought that in 7136 Al alloy, the spheroidization of $MgZn_2$ precipitates was due to the change of orientation between precipitates and matrix, thus changing their interface energy. Our previous investigation [33] shows that deformation does not change the orientation between precipitates and matrix, nor does it change the composition of precipitates, but alters the dissolution (endothermic enthalpy) and formation (exothermic enthalpy) of precipitates.

In the light of solid phase transformation nucleation theory [34], new interface will be formed between the new phase and the parent phase when the new phase particles are desolved and precipitated. As heat treatment and hot deformation were carried out below solution temperature, the phase composition and crystal structure of α-Al were changed due to the movement of atoms, resulting in the transformation from the state of high Gibbs free energy (dislocation aggregation, strain) to new phase with low Gibbs free energy (such as recovery, precipitation or spheroidization). When 7055 Al alloy is held or deformed below the solid phase line, the solid phase transformation process will occur and $MgZn_2$ phase will be precipitated, which could reduce the Gibbs free energy of the whole system. The reduction of Gibbs free energy ΔG can be expressed as:

$$\Delta G = \Delta G_a + \Delta G_b \tag{3}$$

Where, ΔG_a and ΔG_b can be represented as:

$$\Delta G_a = -V\Delta G_V + V\Delta G_\varepsilon \tag{4}$$

$$\Delta G_b = A\gamma \tag{5}$$

Where V is the volume of the new phase, ΔG_V is the Gibbs free energy difference between the parent phase and the new phase per unit volume (G_{parent}-G_{new}), ΔG_ε is the strain energy of the new phase per unit volume, A is the total surface area of the new phase, and γ is the interface energy between the new phase and the parent phase (assuming no directionality).

In this process, the change of Gibbs free energy ΔG of the whole system is composed of two parts, one is the change of Gibbs free energy ΔG_a caused by chemical free energy for the formation of new phase and strain energy (formula (4)). The former ($V\Delta G_V$) is the driving force of phase transformation, which is negative, and the latter ($V\Delta G_\varepsilon$) is the resistance of phase transition, which is positive. The other part is formation of new interface energy ΔG_b between the parent phase and the new phase. To form new phase, energy working must be done to counteract ΔG_b, resulting in increased free energy of the whole system, so it is a positive value of ΔG_b.

During heat treatment and hot deformation of 7055 Al alloy, the precipitation of new phase is also determined by the change of Gibbs free energy of the whole system ΔG. The new precipitates are mainly $MgZn_2$ particles. The interfacial energy ΔG_b formed between the parent phase and the new phase is related to the size and density of precipitates. The main driving force ΔG_a for the new phase to precipitate is related to ΔG_V. The new phase here is relatively simple (mainly $MgZn_2$ phase). Under the process of over aging heating and hot deformation, Gibbs free energy changes due to absorption of deformation energy. In other words, numerous defects (e.g., dislocations) accumulate to form deformation storage energy, which changes the Gibbs free energy difference between $MgZn_2$ phase and Al matrix.

Figure 9 is the schematic diagram of deformation induced precipitation process. When SQ-7055 was over aged at 300 °C, the concentration of $MgZn_2$ in the parent phase changed due to the decreased solubility (figure 1(b)). From the thermodynamic point of view, the structure of high Gibbs free energy state will change to low Gibbs free energy state (new phase precipitation), so new phase nucleated and grew at grain boundaries (GBPs) and in grain interior (MPts) as shown in figure 9(b). In polycrystals, grain boundaries will become channels for the rapid diffusion of atoms and easily cause the segregation of Mg and Zn atoms, thus forming $MgZn_2$ phase. $MgZn_2$ nucleates and grows preferentially at grain boundaries. Therefore, GBPs are coarser than MPts and continuously distributed (figures 6(b) and 9(b)).

After over aging treatment, 7055 Al alloy was subjected to hot compression. A great quantity of defects (e.g., dislocations) were introduced (figure 9(c)). These defects with large fluctuation will become the short-circuit

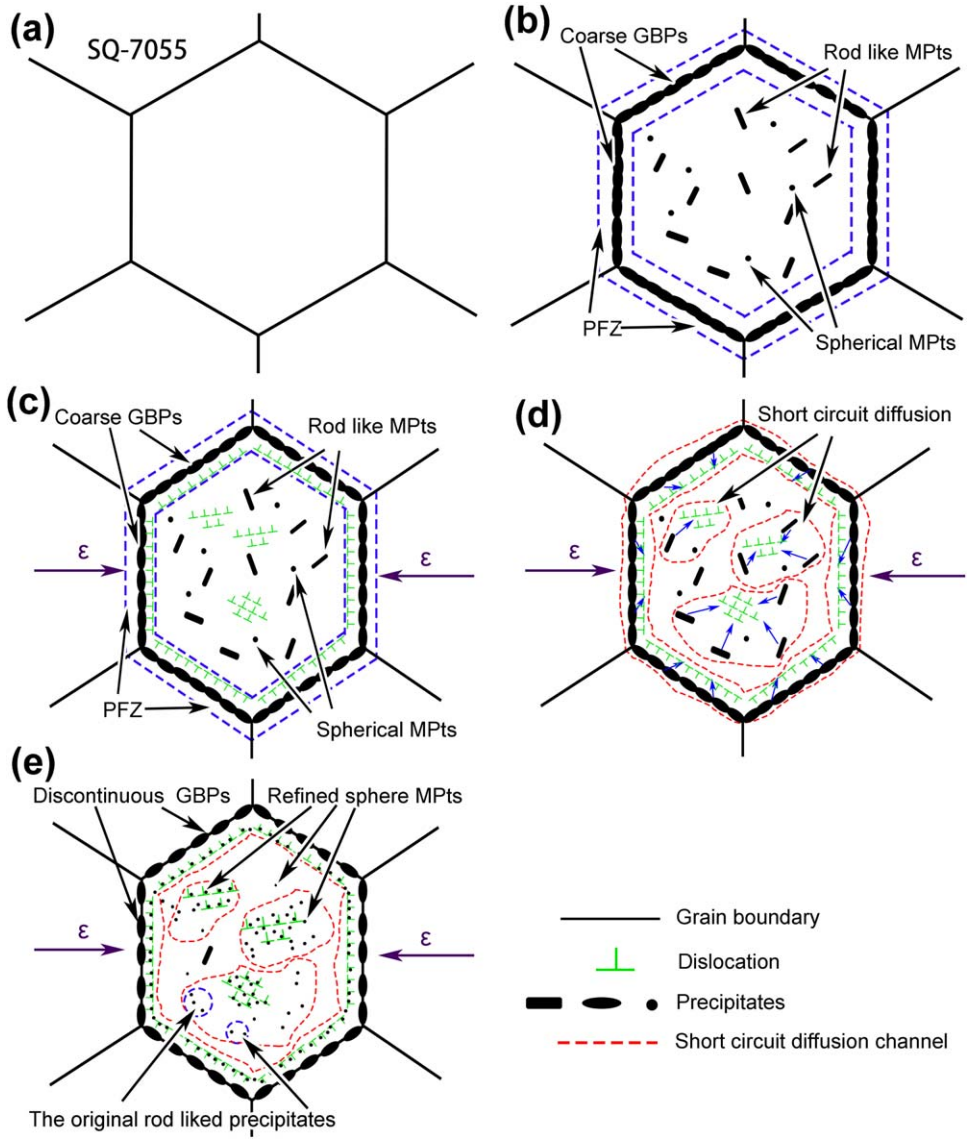

Figure 9. Schematic diagram of deformation induced precipitation process: (a) SQ-7055; (b) over aged; (c) deformed; (d) Short circuit diffusion of atoms; (e) The final morphology of DIPs.

diffusion channels for solute atoms and accelerate their diffusion (figure 9(d)). Simultaneously, these defects change the original chemical potential in the grains, thus altering the diffusion direction and segregation position of Mg and Zn atoms ((figure 9(d))).

When new phase nucleates at these defects, the defects will disappear or be destroyed, thus releasing a part of energy, reducing the total Gibbs free energy ΔG of the system and stabilizing microstructures [35]. The heterogeneous nucleation increases the quantity of nucleation sites for precipitates and the interfacial energy ΔG_b.

Of all the shapes, Gibbs free energy of the spherical precipitates is the lowest leading more stable system. The change of Gibbs free energy during dynamic precipitation can be described by the formula as follows [34, 36]:

$$\Delta G' = -V\Delta G_V + V\Delta G_\varepsilon + A\gamma - V\Delta G_D \tag{6}$$

Where ΔG_D is the decrease of Gibbs free energy per unit volume after nucleation at defects. The critical nucleation radius R^* can be expressed as [34, 36]:

$$R^* = 2\gamma/(\Delta G_V + \Delta G_\varepsilon + \Delta G_D) \tag{7}$$

It can be seen from formula (6), (7) that with the increased deformation, ΔG_D increases, leading to the denominator $(\Delta G_V + \Delta G_\varepsilon + \Delta G_D)$ increasing. The critical nucleation radius R^* decreases and the driving force of precipitation $\Delta G'$ increases, resulting in increased nucleation ratio and nucleation quantity. Therefore, the size of precipitates decreases with deformation (figures 8 and 9(e)). As a result, the interfacial energy per unit volume of the new phase (γ) increases. The effect of interface energy on nucleation gradually exceeds that of

strain energy (ΔG_ε) and plays a leading role. Moreover, the interfacial energy of spherical particles is the lowest, so strain makes $MgZn_2$ precipitates spheroidize to reduce the Gibbs free energy of the system. Therefore, in this experiment, the morphology of deformation induced precipitates are spherical (figures 8 and 9(e)).

The desolvation and precipitation of second phase particles is essentially diffusion and segregation of solute atoms. Deformation induces defects (e.g., sub grain boundaries, dislocations and vacancies). The region near these defects is distorted with high energy. Alloying elements (Mg, Zn, etc) interact with these defects and enrich in the region near these defects, which is called atom clustering. As a result, these defects change the diffusion direction of atoms (new region of segregation). The diffusion of partial solute atoms of the rod-shaped precipitates to the new segregation position can also be regarded as a special re-dissolution and re-precipitation process.

According to the explanation of PFZ in section 3.2, grain boundary structure is loose, which is a channel for the rapid diffusion of atoms in polycrystalline, and it is easy to cause the segregation of solute atoms. There are many defects such as vacancies on grain boundaries, which make it in the state of stress distortion, so the energy is high. Grain boundary become the preferential nucleation region during solid phase transformation [22]. Therefore, the concentration of vacancy and solute in the region near grain boundaries is lower than the critical nucleation condition. A great deal of dislocations were introduced during hot deformation of 7055 Al alloy. Dislocation movement is hindered by grain boundaries. When the force to move dislocations is equal to the drag force of grain boundaries, dislocations stop and block in front of grain boundaries. This is the so called dislocation stacking [37]. These dislocations in the vicinity of grain boundaries decrease the chemical potential in the region and become a channel for the rapid diffusion of atoms, thus reducing the width of PFZ (figures 8(f) and 9(e)).

In this paper, the following conjecture were proposed: mass defects (such as vacancies, dislocations, etc) introduced by hot deformation can accelerate the diffusion and segregation of solute atoms, causing deformation induced precipitation. Based on the theory of desolvation and nucleation, the strain energy is dominant and precipitates are rod like under over aging or low deformation. While the interface energy is dominant and the precipitates are fine spherical with increased deformation. However, in the practice industrial production (such as hot rolling, hot extrusion, hot forging, etc) many kinds second phase of different shapes exist for various alloys especially heat-treatable aluminium alloys after hot deformation. The key is that precipitation is also related to the dynamic process apart from the thermodynamic condition which can only provide the final state of certain phase at equilibrium state.

4. Conclusion

In this paper, the influence of strain parameters on grain structure and precipitates of 7055 Al alloy were studied in detail. The conclusions can be summarized as follows:

(1) After double-step solution treatment, some coarse equiaxed grains were formed, but the elongated deformed grains were still dominant. The strengthening phase $MgZn_2$ completely dissolved into matrix, while the high melting point coarse second phase particles (e.g., Al_7Cu_2Fe and Al_2CuMg) hardly changed.

(2) After over aging at 300 °C, particles preferentially precipitated at grain boundaries. Size, quantity and volume fraction of precipitates increased with increased over aging time. However, after 120 s, the growth rate became slow, and the morphology of precipitates also changed. The quantity of spherical precipitates decreased with rod-shaped precipitates increased.

(3) After hot compression, grains of 7055 Al alloy were elongated and a large amount of DIPs were formed. The grain width increased with increasing deformation temperature and decreasing deformation rate. However, with the increase of deformation, grain width first decreased and then increased, the minimum value was taken at 60%. Due to the effect of deformation induced spheroidization and refinement, the size of precipitates decreased with the increase of deformation and gradually spheroidized.

Acknowledgments

This research is supported by the Natural Science Foundation of Zhejiang (No. LQ19E010003), Ningbo Natural Science Foundation (No. 202003N4082), projects in Science and Technique Plans of Ningbo City (No. 2019B10100), the Major State Research and Development Program of China (No. 2016YFB0300801), the State Key Laboratory for Advanced Metals and Materials of China (No. 2019-Z16), and Sponsored by the K.C. Wong Magna Fund in Ningbo University.

ORCID iDs

Jinrong Zuo https://orcid.org/0000-0003-3023-6818

References

[1] Kumar V M and Venkatesh C V 2019 A comprehensive review on material selection, processing, characterization and applications of aluminium metal matrix composites *Mater. Res. Express* **6** 72001
[2] Li H, Zhu Z F and Y Z H 2018 Hot deformation characterization of a novel Al–Zn–Mg–Cu aluminum alloy through processing map and microstructure evolution *Mater. Res. Express* **5** 066522
[3] Gu K, Wang K, Chen L, Guo J, Cui C and Wang J 2019 Micro-plastic deformation behavior of Al–Zn–Mg–Cu alloy subjected to cryo-cycling treatment *Mat. Sci. Eng.* A **742** 672–9
[4] Peng X, Su W, Xiao D and Xu G 2018 Investigation on hot workability of homogenized Al–Zn–Mg–Cu alloy based on activation energy and processing map *JOM* **70** 993–9
[5] Jang B J, Park H S and Kim M S 2018 High temperature deformation behavior of Al–Zn–Mg-based new alloy using a dynamic material model *Met. Mater. Int.* **24** 1249–55
[6] Xu X J *et al* 2019 Microstructural evolution and mechanical properties of Al–Zn–Mg–Cu alloy processed by integrated extrusion and equal channel angular pressing (iECAP) and heat treatment *Mater. Res. Express* **6** 0865b8
[7] Oko O E, Mbakaan C and Barki E 2020 Experimental investigation of the effect of processing parameters on densification, microstructure and hardness of selective laser melted 7075 aluminium alloy *Mater. Res. Express* **7** 036512
[8] Zhao J, Deng Y, Tang J and Zhang J 2019 Influence of strain rate on hot deformation behavior and recrystallization behavior under isothermal compression of Al–Zn–Mg–Cu alloy *J. Alloy. Compd.* **809** 151788
[9] Wert J A *et al* 1981 Grain refinement in 7075 aluminum by thermo-mechanical processing *Metall. Mater. Trans.* A **12** 1267–76
[10] Cardoso K R *et al* 2011 High strength AA7050 Al alloy processed by ECAP: microstructure and mechanical properties *Mat. Sci. Eng.* A **528** 5804–11
[11] Zuo J R, Hou L G, Shu X D, Peng W F, Yin A M and Zhang J S 2020 Grain refinement assisted by deformation enhanced precipitates through thermomechanical treatment of AA7055 Al alloy *Metals* **10** 594
[12] Dang P *et al* 2009 Evolution of precipitates in Al-Cu alloy subjected to equal-channel angular pressing *Mater. Sci. Tech-Lond.* **17** 263–9
[13] Peng B S *et al* 2009 Dissolution behavior of second phases in Al-Cu binary alloy during severe plastic deformation *Chin. J. Nonferrous. Met.* **19** 874–80
[14] Zhang Z Z *et al* 2009 Reprecipitate behavior of supersaturated solid solution of Al-Cu alloy caused by severe plastic deformation during subsequent deformation *Chin. J. Nonferrous. Met.* **19** 1962–8
[15] Yu Y N and Liu G Q 1989 *Principle and Application of Stereological Quantitative Analysis* (Beijing: Metallurgical Industry Press) 35–40
[16] Robson J D 2004 Microstructural evolution in aluminium alloy 7050 during processing *Mat. Sci. Eng.* A **382** 112–21
[17] Li X M and Starink M J 2001 Effect of compositional variations on characteristics of coarse intermetallic particles in overaged 7000 series aluminium alloy *Mater. Sci. Tech-Lond.* **17** 1324–8
[18] Knipling K E *et al* 2006 Criteria for developing castable, creep-resistant aluminum-based alloys-a review *Z. Metallkd* **97** 246–65
[19] Duan Y B, Tang J and Zeng S M 2003 Effect of interstage homogenizing treatment on homogenization degree and overburnt temperature of 7A04 alloy *Aluminum Fabrication* **03** 23–6
[20] Angella G *et al* 2006 Microstucture evolution and aging kinetics of Al–Mg–Si and Al–Mg–Si–Sc alloys processed by ECAP *Mater. Sci. Forum* **503-504** 493–8
[21] Chen C Q and Knott J F 1981 Effects of dispersoids particles on toughness of high-strength aluminium alloys *Met. Sci.* **15** 357–64
[22] Tian R Z and Wang Z T 2000 *Handbook of Aluminium Alloy and its Working* 1st edn (Changsha, China: Central South University Press) pp 250–2
[23] Schmuck C *et al* 1995 Quantitative analysis of GP zones formed at room temperature in a 7150 Al-based alloy *Appl. Surf. Sci.* **87-88** 228–33
[24] Zuo J R *et al* 2017 Enhanced plasticity and corrosion resistance of high strength Al–Zn–Mg–Cu alloy processed by an improved thermomechanical processing *J. Alloy. Compd.* **716** 220–30
[25] Ogura T, Hirosawa S and Sato T 2004 Quantitative characterization of precipitate free zones in Al–Zn–Mg(–Ag) alloys by microchemical analysis and nanoindentation measurement *Sci. Tech. Adv. Mater.* **5** 491–6
[26] Sitdikov O 2009 Temperature effect on fine-grained structure formation in high-strength Al alloy 7475 during hot severe deformation *Mat. Sci. Eng.* A **516** 180–8
[27] Chang C S T and Duggan B J 2010 Relationships between rolled grain shape, deformation bands, microstructures and recrystallization textures in Al-5%Mg *Acta Mater.* **58** 476–89
[28] Troeger L P and Starke E A Jr 2000 Particle-stimulated nucleation of recrystallization for grain-size control and superplasticity in an Al–Mg–Si–Cu alloy *Mat. Sci. Eng.* A **293** 19–29
[29] Zuo J R *et al* 2017 The mechanism of grain refinement and plasticity enhancement by an improved thermomechanical treatment of 7055 Al alloy *Mat. Sci. Eng.* A **702** 42–52
[30] Lin Y C *et al* 2015 Effects of pre-treatments on aging precipitates and corrosion resistance of a creep-aged Al–Zn–Mg–Cu alloy *Mater. Des.* **83** 866–75
[31] Nam C Y *et al* 2003 Effect of precipitates on microstructural evolution of 7050 Al alloy sheet during equal channelangular rolling *Mat. Sci. Eng.* A **347** 253–7
[32] Sha G *et al* 2009 Influence of equal-channel angular pressing on precipitation in an Al–Zn–Mg–Cu alloy *Acta Mater.* **57** 3123–32
[33] Zuo J R *et al* 2017 Effect of deformation induced precipitation on dynamic aging process and improvement of mechanical/corrosion properties AA7055 aluminum alloy *J. Alloy. Compd.* **708** 1131–40
[34] Liddicoat P V *et al* 2010 Nanostructural hierarchy increases the strength of aluminium alloys *Nat. Commun.* **1** 63
[35] Doherty R D 1996 Physical metallurgy *Physical Metallurgy* ed R W Cahn and P Haasen (Oxford: North-Holland) pp 1363–505
[36] Lang Y 2012 Grain refinement of 7050 aluminum alloy and its mechanical behavior by hot deformation based on strain-induced precipitation *PhD Thesis* University of Science and Technology Beijing, China
[37] Yu Y N 2000 *Principles of Metallurgy* (Beijing: Metallurgical Industry Press) pp 481–90